ACS Catalysis

pubs.acs.org/acscatalysis
Research Article

Pursuing the Complete OFF State in Photoswitchable Catalysis

Mykola Kravets, Matteo Flaibani, Magdalena Szewczyk, Paola Posocco,* and Volodymyr Sashuk*

Cite This: ACS Catal. 2023, 13, 15967−15976
Read Online

ACCESS | Metrics & More | Article Recommendations | Supporting Information

ABSTRACT: Practically, all photoswitchable catalysts exhibit residual activity in the OFF state. Herein, we present a ruthenium initiator with a built-in photoswitch whose metathetical performance is completely shut off by light. The system is made of Hoveyda−Grubbs second-generation complexes appended, along with background ligands, to a gold nanoparticle surface via azobenzene linkers. Under dark or visible light—the precatalysts, in the presence of an olefin, undergo initiation, diffuse from the surface into bulk solution, and commence metathesis reaction. When the conditions are changed to ultraviolet, the isomerization of the azo switches takes place, burying the precatalysts within the bulky organic monolayer, thus preventing their initiation and thereby halting the reaction. Despite the irreversibility of the process, this work opens up opportunities for the remote deactivation of catalysts without their chemical decomposition and control of more complex tasks such as chemical selectivity.

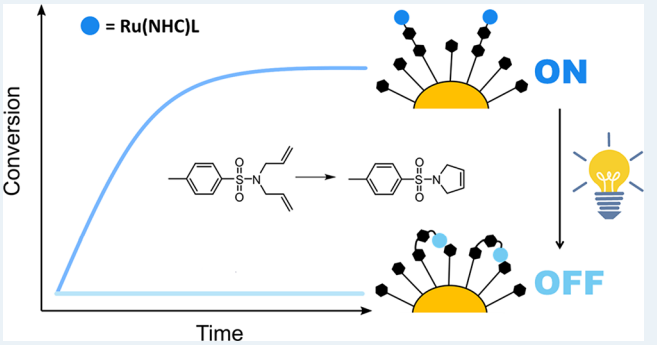

KEYWORDS: *photoswitchable catalysis, azobenzene, ruthenium, Grubbs-Hoveyda complex, olefin metathesis, gold nanoparticles*

INTRODUCTION

Having control over catalysis has long intrigued the scientific community. This eventually spawned an entire discipline called switchable catalysis. While in nature, the catalysis is successfully upregulated and downregulated by complex feedback loops,[1] control in synthetic systems is realized using rather simple chemical or physical stimuli.[2] In this context, the particularly attractive stimulus is light, which is noninvasive, and can be delivered with high spatiotemporal precision.[3] On the other hand, light is not as efficient as a chemical input that can completely stop the reaction.[4] During past decades, researchers have explored miscellaneous approaches to increase the switching efficiency of light-responsive catalysts.[5] It was attempted to take advantage of reversible assembling of catalytic units,[6] solubility differences,[7] shielding the active sites,[8] or altering electronic properties.[9] However, none of these approaches was able to completely suppress the catalytic activity. Regardless of the approach used, the outcome was always the same: either not all of the catalyst has undergone light-induced transformation, the transformed catalyst was less but also active, or there was an active cocatalyst that remained. Here, we show a solution that can cause a molecular (pre)catalyst to fully lose its activity.

Our approach is based on the recently proposed concept of photoswitchable catalysis on metal nanoparticles.[10] In our preliminary work, we suggested that catalysis could be switched off by burying an active center within an organic monolayer covering these nanoparticles. However, during the preparation of our prototype, we faced the issues typical of other steric approaches (Figures 1A,B). Particularly, when all active sites have been buried, they were still available for catalysis due to the insufficient shield of the underneath monolayer against the incoming substrates.

In the current report, we demonstrate that an external barrier imposed by the monolayer alone is not enough and that additional steric constraints around an active site are necessary to fully disable access to it (Figure 1C). Thanks to that, complete suppression of the catalytic activity can be achieved.

RESULTS AND DISCUSSION

From our initial system, we kept two elements: (i) azobenzene, a transducer of light signal, which through conformational changes is aimed at directing the active site toward either a surface or a solution; (ii) ∼ 3 nm gold nanoparticles (AuNPs, Figure S18) enabling the creation of an organic layer on their surface via strong Au−S bonding. We purposely used small particles to provide a high surface-to-volume Au atom ratio, and thus enable high catalyst loadings. Instead of a model organocatalyst (proline), we introduced a metal-based N-heterocyclic carbene (NHC) complex. This was done because

Received: September 18, 2023
Revised: November 16, 2023
Accepted: November 16, 2023

https://doi.org/10.1021/acscatal.3c04435
ACS Catal. 2023, 13, 15967−15976

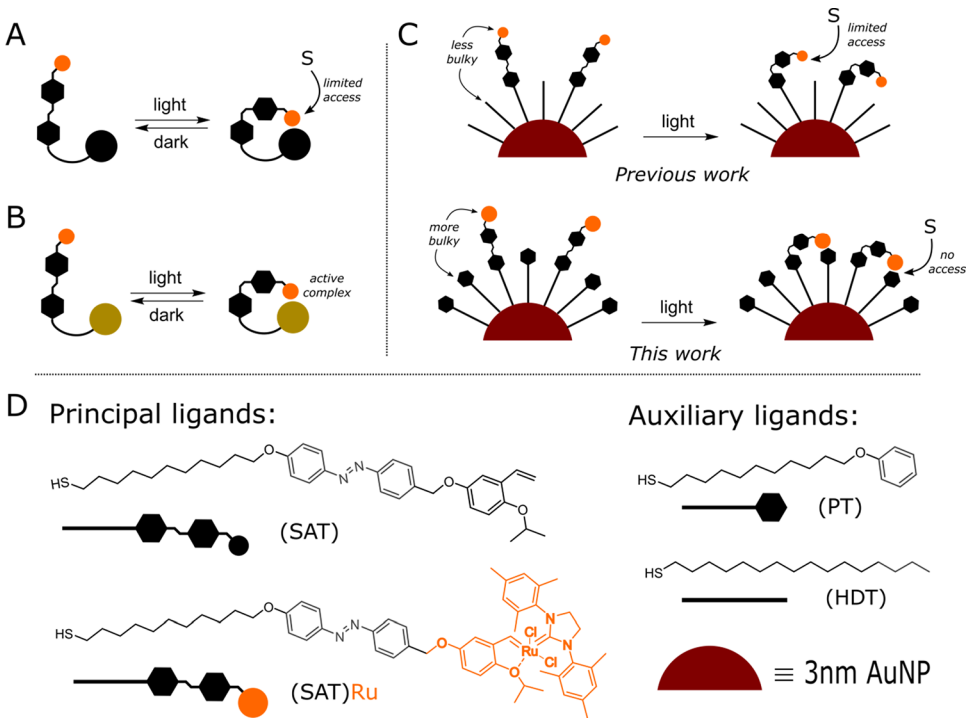

Figure 1. Common steric approaches to control catalysis using photoswitches: (A) shielding the active site using a bulky molecular handle; (B) bringing catalytic units together to create an active complex; (C) our approach based on the regulation of monolayer bulkiness on the nanoparticle surface; and (D) ligands and nanoparticles used in the current study.

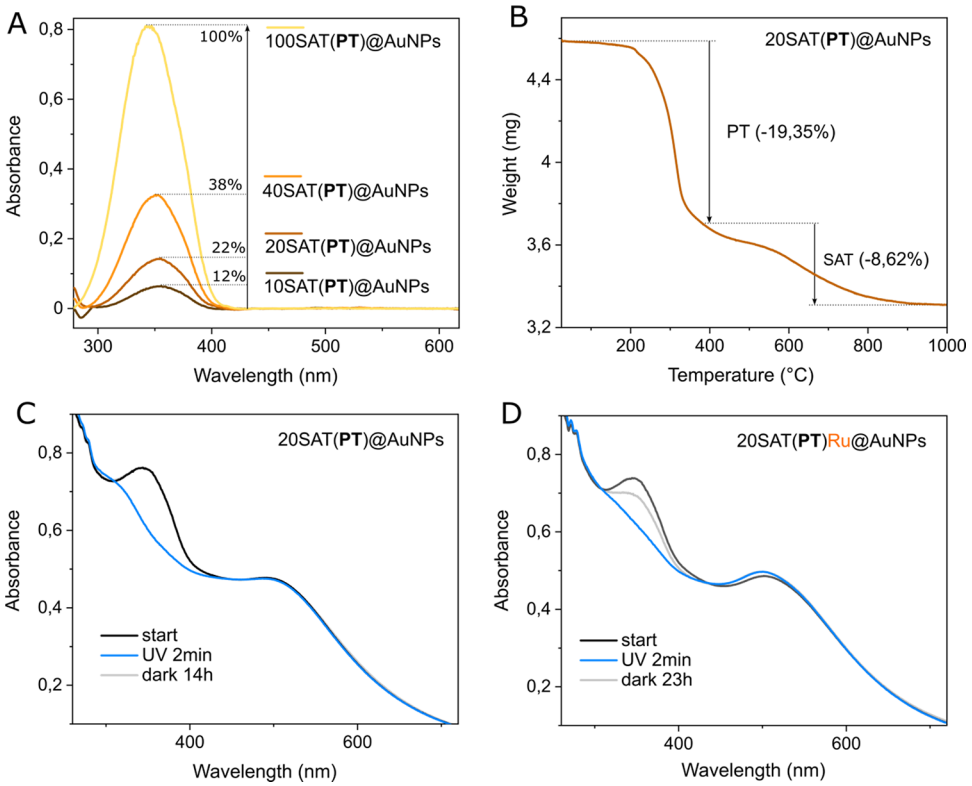

Figure 2. Experimental proof for the presence of SAT ligands on the AuNP surface: (A) absorbance spectra of AuNP dispersions (0.14 mM) with different ligand ratios after the subtraction of plasmon peak revealing the relative percentage of SAT in the monolayer; (B) thermogram of 20SAT(PT)@AuNPs showing two distinct weight loss events corresponding to desorption of PT and SAT ligands; (C,D) absorbance spectra of 20SAT(PT)@AuNPs (0.14 mM) showing the isomerization of immobilized SAT ligands before and after metalation. The resurgence of the 350 peak during back isomerization is attributed to the unmetalated SAT ligands (vide infra).

https://doi.org/10.1021/acscatal.3c04435
ACS Catal. 2023, 13, 15967−15976

NHC complexes in general: (i) possess much higher activity which is crucial in light of a limited number of adsorption sites on the nanoparticle surface; (ii) exhibit much larger and easily modulated—via ligand exchange—coordination sphere; (iii) are much more versatile (wider reaction and selectivity scope), which is essential for extending the system for other applications in the future. Since most metal-catalyzed organic reactions occur in nonpolar solvents, the previously employed hydrophilic oligo(ethylene glycol) chains were replaced by lipophilic hydrocarbon chains. In addition to providing colloidal stability, these spacers, owing to the presence of terminal phenyl groups, were aimed at increasing the interligand spacing (for effective azobenzene isomerization), while providing an overall bulkiness to the monolayer (for effective shielding of active sites).

Initially, we synthesized two ligands: (i) a styrene-azobenzene-thiol (SAT), the principal ligand for supporting the active site; (ii) a phenyl-thiol (PT), the auxiliary ligand for regulating the number of active sites and the relative distance between them on the nanoparticle surface (Figures 1D and S1−S17). The length of PT (∼1.9 nm) was chosen so that ideally it would not protrude beyond the azo bond of adjacent SAT ligands (∼2.1 nm) and interfere with their isomerization on the NP surface. For the decoration of the latter, SAT absorbates were used neat (100%) or mixed with PTs in different molar ratios (10, 20, and 40% of SAT). To ensure a quantitative reaction, the ligands were taken in a total molar amount that is 1.5 times greater than the estimated number of adsorption sites on the NP surface.[10] The NPs employed were stabilized by dodecylamine and surfactant.[11] After agitating the reaction mixtures for 1 h, which was enough for the ligand exchange,[12] the unreacted materials were washed out by multiple dissolution−precipitation of the NP residues. The purified NPs were dispersed in DCM to give 7 mM colloidal solutions. The successful adsorption of SAT ligands was confirmed by the appearance of $\pi-\pi^*$ transition bands with a maximum at 350 nm belonging to the *trans* form of azobenzene. After the subtraction of the plasmon resonance, the intensities of these bands (0.063, 0.142, 0.323, and 0.764 au) were found to be nearly proportional to the amount of SAT ligands in the feed mixtures (10, 20, 40, and 100%), indicating that both ligands were coadsorbed and that the initial ratios were preserved (Figure 2A).

Hereafter, the obtained NPs are termed χSAT(**PT**)@AuNPs, where χ is the mole percentage of SAT in the feed mixture. Additionally, to confirm the accordance of the ligand ratio on the surface with that in solution, we have prepared a ∼4.6 mg batch of colloidally stable 20SAT(**PT**)@AuNPs (vide infra) and performed ligand desorption using thermogravimetry (Figure 2B). We also recorded a thermogram for particles coated exclusively with background ligands (Figure S19) to distinguish weight loss caused by PT desorption from weight loss caused by SAT and estimate the percentage of the latter in the mixed monolayer, obtaining ∼18%, which is very close to the theoretical value (20%) and that (22%) determined from the absorbance spectra (Figure 2A).

In the next step, we investigated the isomerization of the SAT ligands. The conversion from the thermodynamically favored *trans* form to the less stable *cis* form was carried out in a fluorimeter chamber by irradiating the prepared samples using a built-in xenon arc lamp with a light of the wavelength of 365 nm and bandwidth of 20 nm. The degree and rate of the isomerization were assessed based on absorbance spectra (Figure S27). The photostationary state for all samples was achieved within 2 min. Similarly to unbound SAT (Figures S25−S26), the $\pi-\pi^*$ transition band dropped to the background, suggesting almost complete isomerization. Spontaneous reverse isomerization occurring in the dark was also quantitative but took much longer (up to 150 min) with a clear dependence: the higher the content of SAT, the faster the process (Figure S30).

In an attempt to gain more details on the dependence of the back isomerization rate from χ, we performed atomistic simulations on these nanoparticles (see SI for details). They were simulated with SAT ligands in the *trans* conformation first and then reverted to *cis* in order to follow the same experimental pathway. The so obtained equilibrated molecular structures are reported in Figure S45. By means of umbrella sampling calculations (US) (see SI), we then computed the free energy barrier for the *cis* → *trans* isomerization of the CNNC dihedral angle and the NNC angle, the two most significant parameters to investigate azobenzene thermal relaxation.[13] The average value of ∼21 kcal/mol found for all χSAT(**PT**)@AuNPs is comparable to that for the free SAT ligand in DCM (∼20 kcal/mol). This suggests that an increase in the energy barrier of the CNNC dihedral and the NNC angle due to steric hindrance at the nanoparticle surface is likely not the primary reason for the (low) composition-dependent back isomerization observed in the experiments. Another possible explanation may be that SAT reverse isomerization is being aided by *trans* neighboring SAT ligands. Such a collective switching behavior has been already proposed in the past;[14] our current calculations found no indication of a quantitative difference either in the energy (∼20 kcal/mol) and in the pathway for SAT reverse isomerization when all neighboring ligands are already in the *trans* state (Figure S46). This point demands further exploration and more sophisticated models.

Notably, after accomplishing the full switching cycle, only the sample with 20% SAT returned to the pristine spectrum (Figure 2C); whereas the spectra of the remaining samples have undergone slight changes in the line shape with the noticeable increase of the $\pi-\pi^*$ transition band (Figure S27). The observed increase is most likely accounted for changes in the dielectric function of the monolayer caused by AuNP aggregation manifested by the broadening of the plasmon resonance and eventually the emergence of a new peak over time (Figure S28).

Having scrutinized the isomerization behavior of SAT ligands, we proceeded to install active sites. We chose a Hoveyda−Grubbs second-generation ruthenium complex (**H2**) in which the active site is encompassed by bulky mesityl rings. Because of the danger of poisoning the metal center with the sulfur of thiol group,[15] the precatalyst was generated in situ in the reaction between the styrene moieties of the adsorbed SAT ligands and a commercial Grubbs second-generation ruthenium complex (**G2**). The reaction was performed in the presence of copper(I) chloride to shift the equilibrium toward the product by catching the releasing phosphine. Both **G2** and CuCl were employed in equimolar amounts in respect to the adsorbed **SAT** ligands. Considering the steric constraints within the monolayer, the reaction time was set as 2 h, which is at least twice as long for the analogous reaction to occur in solution. The incorporation of the ruthenium onto the surface was monitored by the temporal evolution of the $\pi-\pi^*$ transition band of 20SAT(**PT**)@AuNPs, which showed the

https://doi.org/10.1021/acscatal.3c04435
ACS Catal. 2023, 13, 15967−15976

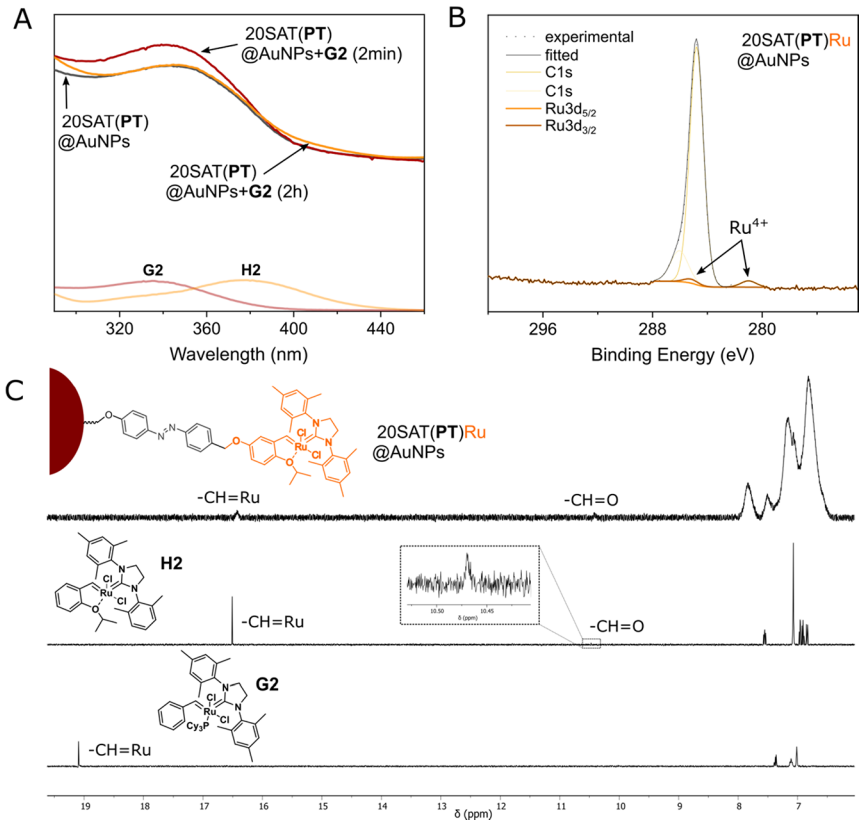

Figure 3. Experimental evidence for ruthenium insertion into the SAT ligand: (A) temporal evolution of the absorbance spectrum after addition of the **G2** complex to the dispersion of 20SAT(**PT**)@AuNPs. To highlight the spectral changes that occurred during the reaction, normalization procedure was applied and the spectra of unbound **G2** and **H2** were added for comparison; (B) partial X-ray photoelectron spectrum of the modified AuNPs after their purification. A peak at 281 eV was identified as Ru $3d_{5/2}$; (C) partial ^{1}H NMR spectra of the AuNPs with immobilized **H2** and unbound **H2** and **G2** for comparison (DCM-d_2, 293 K), showing the presence of a resonance for vinyl protons coupled with Ru between 16 and 17 ppm characteristic for **H2** complexes.

highest colloidal stability (vide supra). In the initial stage of the reaction, the peak centered at 344 nm increased and moved by ≈6 nm toward the blue region due to the presence of large amounts of unreacted **G2** with a maximum at 336 nm. With the lapse of time, its position began to change eventually settling ≈2 nm to the right of the original position due to overlapping with the emerging signal of **H2** having a maximum at 400 nm (Figure 3A). Similar changes were observed for the remaining samples and were the most pronounced for 100SAT(**PT**)@AuNPs, where the total amount of **H2** formed was expected to be the largest (Figure S23). To further support the generation of **H2** on the surface, a portion of 20SAT-(**PT**)Ru@AuNPs was precipitated with pentane and washed several times with MeOH to remove any unbound ruthenium species. The XPS analysis of the resulting precipitate revealed the presence of Ru^{4+} corresponding to the oxidation state of the metal (Figure 3B) as well as other heteroatoms present in **H2** complex (Figure S20). The obtained sample was then examined by NMR spectroscopy, which showed the appearance of a broad singlet resonance at 16.42 ppm attributed to the −CH═Ru proton of the immobilized **H2** (Figure 3C). Another characteristic signal was observed at 10.41 ppm, which most probably belongs to the product of its solvolysis (−CH═O)[16] and is also present in unbound **H2**, albeit in much less amount, suggesting that MeOH used during the NP purification speeds up the degradation process. Furthermore, the integration of these two proton resonances (Figure S21) revealed that only 39% of absorbed SAT ligands underwent metalation reaction; while the comparison of other integrals showed the total percentage of SAT ligands in the monolayer as 25%, which is in line with the previous findings (vide supra). Given the incomplete reaction with **G2**, the obtained NPs are further denoted as χSAT(**PT**)Ru@AuNPs, indicating only the content of the SAT ligand.

After introducing the active sites, we began the isomerization experiments (Figure S29). We have not noticed that the enlargement of the SAT ligand greatly influenced its capability of converting to the *cis* form. The isomerization was as fast as before and lead to the disappearance of the $\pi-\pi^*$ transition band. The situation has, however, changed when the process of returning to *trans* form was triggered. While the trend of increasing the rate with the number of SAT ligands persisted, the overall process was much slower and incomplete (Figure S30). The lowest conversion (52%) was obtained for the sample with the lowest (10%) SAT coverage, and the highest conversion (79%) was achieved for the sample fully covered with SAT (100%). In addition, we found that the amount of "unreturned" ligands (37%, the colloidally stable sample with 20% SAT) correlates with the amount of the attached **H2** complex (39%, vide supra). These results, in addition to confirming the presence of bulky ruthenium termini, indicated that some interactions between Ru and the monolayer are established during the *trans*-to-*cis* isomerization, preventing the metalated SAT ligands from returning to the initial state once the light source was removed.

https://doi.org/10.1021/acscatal.3c04435
ACS Catal. 2023, 13, 15967−15976

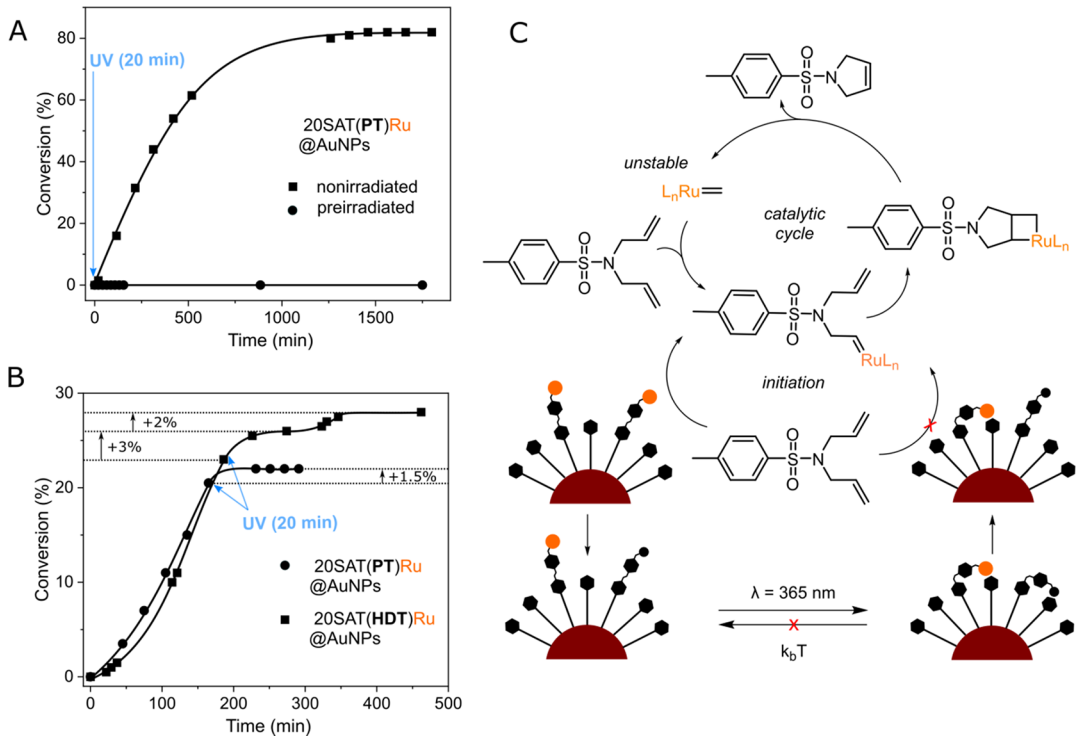

Figure 4. Catalytic experiments: (A) time−conversion plots for metathesis reaction occurring in nonirradiated and preirradiated CH_2Cl_2-d_2 solutions containing olefin (4 mM) and 20SAT(PT)Ru@AuNPs (10% mol in terms of SAT ligand); (B) time−conversion plots for metathesis reaction carried out first in the dark, then under UV light, and again in the dark, catalyzed by Ru containing 20% SAT AuNPs that differed in the type of background ligand; (C) plausible mechanism of the initiation and catalysis of metathesis reaction in the presence of Ru containing AuNPs with PT as background ligand. The initiation leads to the generation of AuNPs with a reduced amount of Ru precatalysts that get stuck in the monolayer after irradiation and are not able to reinitiate the catalytic cycle (in contrast to AuNPs with HDT, where partial reinitiation takes place).

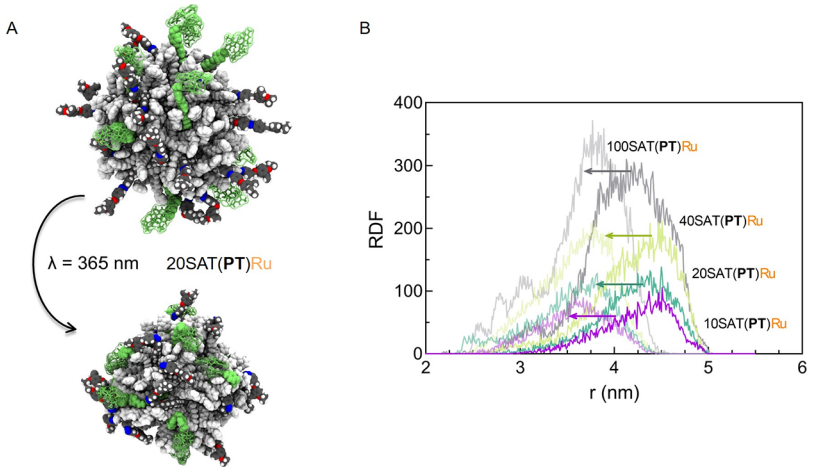

Figure 5. (A) Molecular structure of 20SAT(**PT**)Ru@AuNPs extracted from its equilibrated atomistic simulations in DCM (not shown). All SAT ligands are initially in their *trans* conformation (top) and then reverted to *cis* (bottom). SAT chains are colored by element (C, gray; N, blue; O, red, H, white), with those presenting the catalytic group in green, and PT chains are portrayed as white spheres. The Hoveyda-Grubbs moiety is highlighted as a green transparent surface. (B) Radial distribution function (RDF) of the Ru atom calculated from the gold surface for each monolayer composition χ (10, 20, 40, and 100). Dark curves, *trans* state; light curves, *cis* state.

Having obtained the proof of the isomerization of the metalated SAT, we moved on to testing the nanoparticles in catalysis. As a model reaction, we took the ring-closing metathesis of *N*,*N*-diallyltosyl amide. First, the reaction was carried out in the dark, that is, when the catalytic units are expected to be revealed to solution. Since the actual amount of "active" ruthenium in each sample was difficult to quantify, we varied the amount of the substrate to maintain the amount of both metalated and unmetalated SAT ligands at 10 mol %. We found that each sample displayed very different activity (Figures 4A and S33−S36, S41). The NP dispersions with 10% SAT were the least active. Those containing 20 and 40% SAT were practically indistinguishable. While the sample with 100% SAT was enormously active. These results confirmed our preliminary conclusion that the amount of **H2** generated in each sample is different and indicated that the unreacted **G2**,

https://doi.org/10.1021/acscatal.3c04435
ACS Catal. 2023, 13, 15967−15976

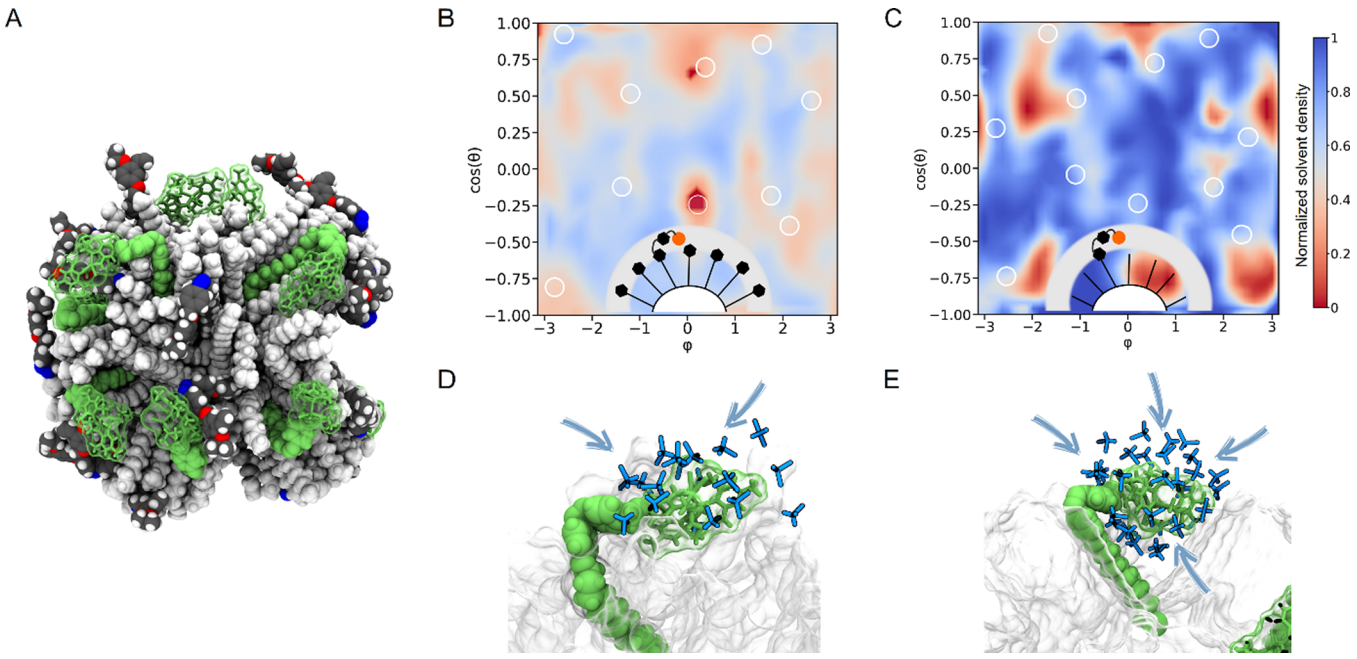

Figure 6. (A) Molecular structure of 20SAT(**HDT**)Ru@AuNPs extracted from equilibrated atomistic simulations in DCM (not shown). All SAT ligands are in the *cis* state. SAT chains are colored by element (C, gray; N, blue; O, red, H, white), with those presenting the catalytic group in green, and HDT chains are portrayed as white spheres. The Hoveyda−Grubbs moiety is highlighted as a green transparent surface. (B,C) Density distribution of the solvent at the distance from the gold core where the catalytic group is most often placed during the simulation time: (B) 20SAT(**PT**)Ru@AuNPs and (C) 20SAT(**HDT**)Ru@AuNPs. White circles identify the position of the Ru atom. The distribution is shown as a two-dimensional projection of the sphere surface (*x*-axis, the azimuthal angle φ; *y*-axis, the cosine of the polar angle θ) and is normalized on the density of the solvent in bulk. Red areas represent poorly solvated regions (e.g., less accessed), while blue areas highly solvated regions (e.g., highly accessed). (D, E) Visual comparison of solvent molecules in close contact (in blue) with the precatalytic group in 20SAT(**PT**)Ru@AuNPs (D) and 20SAT(**HDT**)Ru@AuNPs (E), showing one SAT(Ru) ligand (in green) as a representative example. The same pictures, but before the *trans* → *cis* transformation occurs, are reported in Figure S49.

which is much more active than **H2**, is present in the sample with full SAT coverage, which is most likely concerned with the access of **G2** complex to styrene moieties within variously composed monolayers (the hindered access to the monolayer is also evidenced by the different speed of the reaction catalyzed by free and immobilized H2, Figure S42B). The above assumptions were further supported by catalytic studies conducted under UV light. The NP dispersions (5.6 mM) were first irradiated and then subjected to the substrate. In view of the higher NP concentration (when compared to UV−vis studies), the irradiation time was elongated to ≈20 min to ensure complete isomerization. As anticipated, whereas the NPs covered with 100% of SAT displayed some residual activity (due to the presence of **G2** remnants), the other samples had no activity at all. Experiments with the immobilized Ru precatalyst without the azobenzene fragment (20ST(**PT**)@AuNPs, Figure S22) confirmed that the observed catalyst deactivation is due to the physical concealment of ruthenium centers within the created monolayers and not because of decomposition (Figures S37 and S43).

Atomistic simulations also support this. Indeed, monitoring of the ruthenium center during the simulation time revealed a marked shift in the position of the precatalytic group closer to the gold core once the *trans* → *cis* isomerization has occurred. Visual inspection of the molecular trajectories also displays them qualitatively (Figures 5 and S47). In a few cases, the high flexibility of the ligand chains allows the ruthenium centers to even approach the nanoparticle core.

Another factor contributing to the screening of the precatalytic group could be the bulkiness of the background PT ligand, which may offer an additional steric obstacle to diffusion of the substrate when ligands are already converted in their *cis* state. To verify this hypothesis all PT ligands were replaced by aliphatic ligands (1-hexadecanethiol, HDT). From molecular calculations, we see that the lack of the terminal phenyl ring in HDT ligands enables stronger and persistent interactions between the alkyl portions of the chains,[17] leading to clustering of ligands. The nonuniform distribution of the chains on the surface makes the monolayer locally more exposed to the external environment (Figures 6 and S48). This consequently has an impact on the level of exposure of the precatalytic group to the outside.

A simple yet effective way to indirectly verify that is by quantifying the accessibility of the group by estimating the average number of solvent molecules encountered by the active site during the simulation time.[18] Figure 6 compares the tridimensional distribution of the solvent molecules around 20SAT(**PT**)Ru@AuNPs (panel B) and 20SAT(**HDT**)Ru@AuNPs (panel C) at a distance from the gold core where the catalytic group is at its highest concentration (see Figure 5B for reference). The values are then normalized to the density of the solvent in the bulk, thus providing a measure of the local solvation of the monolayer. It is apparent that the presence of a bulky group in the background ligand considerably reduces the amount of solvent that is able to diffuse within the organic shell. For 20SAT(**PT**)Ru@AuNPs, this value is always lower than 0.6, meaning that there is a decrease of more than 40% in the local solvation when compared to the bulk solvent. Differently, the distribution is far from uniform in 20SAT-(**HDT**)Ru@AuNPs, with regions where DCM molecules are

https://doi.org/10.1021/acscatal.3c04435
ACS Catal. 2023, 13, 15967−15976

not detected (i.e., inside ligand bundles) and regions where the solvation is almost identical to that of the bulk solvent (i.e., between two ligand clusters). Considering specifically the position of the Ru atoms (Figure 6, white circles), in 20SAT(**PT**)Ru@AuNPs most of them are placed in a poorly solvated area, which implies that the precatalytic moieties are more difficult to access by the solvent and by other incoming molecules (Figure 6D). Instead in 20SAT(**HDT**)Ru@AuNPs they can be found close to blue regions on the map, so they are well exposed to the solvent and easily accessible from the surrounding environment (Figure 6E). Overall, these collective pieces of evidence support the possibility to screen a catalytic headgroup using a dual approach involving ligands possessing photoswitchable abilities together with ligands presenting bulky groups.

Remarkably, the catalysis can be turned off not only before the start of the reaction but also during its course. For demonstration, we chose the NPs with 20% SAT coverage, which among all samples so far exhibited the highest colloidal stability during the isomerization and the best catalytic performance in terms of available SAT ligands. The experiment was commenced in the dark, and when the conversion of the substrate to the product reached ca. 20%, UV light was applied for 20 min (Figures 4B and S38). As expected, the NP activity ceased, albeit not immediately—when the sample was back in the dark. This is because the catalysis does not occur on the surface, but in the solution (Figure 4C). Therefore, it takes a while for catalytic species (L_nRu═), generated from the attached precatalyst and the substrate prior to irradiation, to be deactivated.[19]

Since SAT ligands with time are partially reverted to *trans* forms, we wondered if the NPs would regain their activity. Surprisingly, neither keeping in the dark nor exposing to daylight rendered them active again. This confirmed once again that only ligands containing no ruthenium are able to undergo the reverse isomerization.

To understand the reason for sticking the active centers within the monolayer, we first considered the metathesis between alkene and N═N double bond that could potentially cleave SAT ligand and destroy the precatalyst.[20] However, we did not find any evidence of the formation of the imine product on the NMR spectra (Figures S33−S36). Another reasonable explanation for not returning to the initial state were noncovalent interactions with the underneath monolayer. Initially, we considered $\pi-\pi$ interactions between the mesityl rings of NHC carbenes and phenyl groups of the background ligands. To verify this hypothesis, we synthesized NPs containing 20% SAT, where PT ligands were fully replaced by the aliphatic ligands HDT, denoted as 20SAT(**HDT**)@AuNPs. UV−vis studies revealed that the newly created monolayer SAT ligands (Figure S24) had almost no difficulties with back isomerization when they were devoid of ruthenium and displayed the same slow and incomplete kinetics after metalation (Figures S31 and S32). The only noticeable difference compared to PT monolayers was their catalytic behavior (Figures S40 and S41). Despite the full conversion to the *cis* form, the NPs, albeit much slower, continued to catalyze the reaction after the irradiation was stopped, which agrees with the poorer protection of the active sites by HDT highlighted by the molecular simulations. Moreover, shortly thereafter, the NPs resumed their original activity (Figure 4B), indicating that the immobilized precatalyst serves as a stock for the gradual generation of active species.[19] Our experiments also confirm this, showing that in the case of PT as the background ligand only 52% of the precatalyst is initiated prior to irradiation (Figure S44). The reactivation, however, did not last long. With time, it began to decline, suggesting that HDT, although it enables the metalated SAT ligands to undergo the back isomerization, the extent of the latter is very limited. A similar isomerization and catalytic behavior was also observed when the amount of SAT ligand on the surface was reduced to 10% (Figures S32, S39, and S41). So, we can conclude that $\pi-\pi$ interactions with PT coligands, though theoretically possible, are rather not responsible for the incomplete back isomerization of SAT ligands. Furthermore, the bulkiness of the ruthenium precatalyst is also crucial. This becomes apparent when one compares a light-mediated decrease in catalytic activity of the present system with its prototype,[10] comprising similar linear background ligands, but much smaller proline catalyst units.

It could also be that the nanoconfinement of SAT(Ru) ligands that arises from strong collective local interchain interactions and steric effects due to the bulkiness of the catalytic group hinders the return to the *trans* isomer; by performing US calculations, we reconstructed the free energy surface of the *cis* → *trans* isomerization of the azobenzene in SAT(Ru) along the CNNC dihedral angle. Different local monolayer compositions surrounding a selected SAT(Ru) ligand were considered. However, there was no evidence of an increase in the activation barrier for *cis*-to-*trans* thermal isomerization that could explain the incomplete back isomerization observed in the experiments.

We thus propose the recoordination of Ru atom from the oxygen of the isopropoxyl group to the azo bond of adjacent SAT ligand as the most likely explanation for the incomplete back isomerization. Our previous research suggested that such a bonding should be very strong given the dormant nature of the precatalyst equipped therewith,[21] so potentially being able to hinder the isomerization of the active ligands. This type of interaction can be identified by the appearance of Ru ($4d^6$)-N (π^*) transition around 500 nm.[22] After careful inspection of the absorbance spectra, we indeed noticed a marked shoulder on the left to plasmon peak to appear during the irradiation of the samples with immobilized ruthenium, which does not disappear after the SAT ligands isomerize back to the *trans* forms (Figures 2D, S29, and S31).

CONCLUSIONS

In summary, we have introduced a "double shield" concept for the cessation of catalytic activity. The implementation of this idea, based on a combination of intra- and intermolecular steric constraints for active center screening, was exemplified by the olefin metathesis reaction. The sterically cumbersome ruthenium NHC complex was pinned to the gold nanoparticle surface and directed toward the ligand shell with the aid of an azobenzene photoswitch. When the precatalyst is surrounded by aliphatic ligands, it can access the substrate to some extent and sustain catalysis. However, after terminating these ligands with phenyl rings, the access is blocked, and consequently, catalysis does not take place. The demonstrated ability to remotely stop chemical reactions on demand can be particularly useful for uncontrolled processes, where direct intervention is not possible. Especially, it will be beneficial for controlling chemical selectivity when more than one reaction takes place simultaneously. Current efforts are underway in our

https://doi.org/10.1021/acscatal.3c04435
ACS Catal. 2023, 13, 15967−15976

laboratory to make the process of photoswitching fully reversible, thus enabling cyclic control over catalysis.

■ ASSOCIATED CONTENT

Supporting Information

The Supporting Information is available free of charge at https://pubs.acs.org/doi/10.1021/acscatal.3c04435.

Synthetic procedures; characterization of compounds and nanoparticles (NMR, UV−vis, and MS spectra, TEM, XPS, TGA); isomerization and catalysis kinetics; molecular calculations detail and additional data (PDF)

■ AUTHOR INFORMATION

Corresponding Authors

Paola Posocco − *Department of Engineering and Architecture, University of Trieste, 34127 Trieste, Italy;* orcid.org/0000-0001-8129-1572; Email: paola.posocco@dia.units.it

Volodymyr Sashuk − *Institute of Physical Chemistry, Polish Academy of Sciences, 01-224 Warsaw, Poland;* orcid.org/0000-0002-5907-8596; Email: vsashuk@ichf.edu.pl

Authors

Mykola Kravets − *Institute of Physical Chemistry, Polish Academy of Sciences, 01-224 Warsaw, Poland;* orcid.org/0000-0002-7751-3643

Matteo Flaibani − *Department of Engineering and Architecture, University of Trieste, 34127 Trieste, Italy*

Magdalena Szewczyk − *Institute of Physical Chemistry, Polish Academy of Sciences, 01-224 Warsaw, Poland*

Complete contact information is available at: https://pubs.acs.org/10.1021/acscatal.3c04435

Author Contributions

The manuscript was written through contributions of all authors. All authors have given approval to the final version of the manuscript.

Notes

The authors declare no competing financial interest.

■ ACKNOWLEDGMENTS

The project was financed by the National Science Centre of Poland (grant SONATA BIS 4 no. 2014/14/E/ST5/00778). P.P. and M.F. are particularly grateful to the University of Trieste for financial support; they are also thankful to SISSA for providing access to the ULYSSE cluster and to the CINECA national computing center for computational resources under the ISCRA initiative. We thank Dr. Iwona Misztalewska-Turkowicz, Dr. Agnieszka Wiśniewska, and Dr. Mirosław Krawczyk for TEM, TGA, and XPS measurements, respectively.

■ REFERENCES

(1) Jones, R. *Principles of biological regulation: an introduction to feedback systems*; Elsevier, 2012.

(2) Blanco, V.; Leigh, D. A.; Marcos, V. Artificial switchable catalysts. *Chem. Soc. Rev.* **2015**, *44*, 5341−5370.

(3) Wang, L.; Li, Q. Photochromism into nanosystems: towards lighting up the future nanoworld. *Chem. Soc. Rev.* **2018**, *47*, 1044−1097.

(4) (a) Blanco, V.; Carlone, A.; Hänni, K. D.; Leigh, D. A.; Lewandowski, B. A Rotaxane-Based Switchable Organocatalyst. *Angew. Chem., Int. Ed.* **2012**, *51*, 5166−5169. (b) Yoon, H. J.; Heo, J.; Mirkin, C. A. Allosteric Regulation of Phosphate Diester Transesterification Based upon a Dinuclear Zinc Catalyst Assembled via the Weak-Link Approach. *J. Am. Chem. Soc.* **2007**, *129*, 14182−14183. (c) Biernesser, A. B.; Li, B.; Byers, J. A. Redox-Controlled Polymerization of Lactide Catalyzed by Bis(imino)pyridine Iron Bis(alkoxide) Complexes. *J. Am. Chem. Soc.* **2013**, *135*, 16553−16560. (d) Broderick, E. M.; Guo, N.; Vogel, C. S.; Xu, C.; Sutter, J.; Miller, J. T.; Meyer, K.; Mehrkhodavandi, P.; Diaconescu, P. L. Redox Control of a Ring-Opening Polymerization Catalyst. *J. Am. Chem. Soc.* **2011**, *133*, 9278−9281. (e) Schmittel, M.; De, S.; Pramanik, S. Reversible ON/OFF Nanoswitch for Organocatalysis: Mimicking the Locking and Unlocking Operation of CaMKII. *Angew. Chem., Int. Ed.* **2012**, *51*, 3832−3836.

(5) (a) Dorel, R.; Feringa, B. L. Photoswitchable catalysis based on the isomerisation of double bonds. *Chem. Commun.* **2019**, *55*, 6477−6486. (b) Ihrig, S. P.; Eisenreich, F.; Hecht, S. Photoswitchable polymerization catalysis: state of the art, challenges, and perspectives. *Chem. Commun.* **2019**, *55*, 4290−4298. (c) Majee, D.; Presolski, S. Dithienylethene-Based Photoswitchable Catalysts: State of the Art and Future Perspectives. *ACS Catal.* **2021**, *11*, 2244−2252. (d) Sobczak, G.; Sashuk, V. Photoswitchable Catalysis Mediated by Nanoparticles. *ChemCatChem.* **2021**, *13*, 506−513. (e) Neilson, B. M.; Bielawski, C. W. *Illuminating Photoswitchable Catalysis. ACS Catal.* **2013**, *3*, 1874−1885. (f) Stoll, R. S.; Hecht, S. Artificial Light-Gated Catalyst Systems. *Angew. Chem., Int. Ed.* **2010**, *49*, 5054−5075.

(6) (a) Marcon, M.; Crespi, S.; Pielmeier, A.; König, B. A dinuclear copper(ii) complex with photoswitchable catechol oxidation activity. *Chem. Commun.* **2023**, *59*, 948−951. (b) Ludwig, J.; Helberg, J.; Zipse, H.; Herges, R. Azo-dimethylaminopyridine-functionalized Ni(II)-porphyrin as a photoswitchable nucleophilic catalyst. *Beilstein J. Org. Chem.* **2020**, *16*, 2119−2126. (c) Samanta, M.; Siva Rama Krishna, V.; Bandyopadhyay, S. A photoresponsive glycosidase mimic. *Chem. Commun.* **2014**, *50*, 10577−10579. (d) Krishnan, C. G.; Kondo, M.; Nakamura, K.; Sasai, H.; Takizawa, S. Photoswitchable Chiral Cation-Binding Catalyst: Photocontrol of Catalytic Activity on Enantioselective Aminal Synthesis. *Org. Lett.* **2022**, *24*, 2670−2674. (e) Saha, M.; Bandyopadhyay, S. Reversible photoresponsive activity of a carbonic anhydrase mimic. *Chem. Commun.* **2019**, *55*, 3294−3297. (f) Saha, M.; Hossain, M. S.; Bandyopadhyay, S. A Photoregulated Racemase Mimic. *Angew. Chem., Int. Ed.* **2021**, *60*, 5220−5224. (g) Zhao, Y.; Lei, B.; Wang, M.; Wu, S.; Qi, W.; Su, R.; He, Z. A supramolecular approach to construct a hydrolase mimic with photo-switchable catalytic activity. *J. Mater. Chem. B* **2018**, *6*, 2444−2449. (h) Ma, N.; Li, F.; Li, S.; Chu, S.; Han, L.; Liu, S.; Yan, T.; Tian, R.; Luo, Q.; Liu, J. A remote optically controlled hydrolase model based on supramolecular assembly and disassembly of its enzyme-like active site. *Nanoscale* **2019**, *11*, 3521−3526. (i) Kean, Z. S.; Akbulatov, S.; Tian, Y.; Widenhoefer, R. A.; Boulatov, R.; Craig, S. L. Photomechanical Actuation of Ligand Geometry in Enantioselective Catalysis. *Angew. Chem., Int. Ed.* **2014**, *53*, 14508−14511. (j) Rad, N.; Sashuk, V. A light-gated regulation of the reaction site by a cucurbit[7]uril macrocycle. *Chem. Sci.* **2022**, *13*, 12440−12444. (k) Ueno, A.; Takahashi, K.; Osa, T. Photocontrol of catalytic activity of capped cyclodextrin. *J. Chem. Soc., Chem. Commun.* **1981**, 94−96. (l) Nakamura, K.; Kondo, M.; Krishnan, C. G.; Takizawa, S.; Sasai, H. Azopyridine-based chiral oxazolines with rare-earth metals for photoswitchable catalysis. *Chem. Commun.* **2021**, *57*, 7414−7417. (m) Grill, K.; Dube, H. Supramolecular Relay-Control of Organocatalysis with a Hemithioindigo-Based Molecular Motor. *J. Am. Chem. Soc.* **2020**, *142*, 19300−19307. (n) Niedek, D.; Erb, F. R.; Topp, C.; Seitz, A.; Wende, R. C.; Eckhardt, A. K.; Kind, J.; Herold, D.; Thiele, C. M.; Schreiner, P. R. In Situ Switching of Site-Selectivity with Light in the Acetylation of Sugars with Azopeptide Catalysts. *J. Org. Chem.* **2020**, *85*, 1835−1846. (o) Ren, C. Z.-J.; Solís Muñana, P.; Dupont, J.; Zhou, S. S.; Chen, J. L.-Y. Reversible Formation of a Light-Responsive Catalyst by Utilizing Intermolecular Cooperative Effects. *Angew. Chem., Int. Ed.* **2019**, *58*, 15254−15258. (p) Arif, T.; Cazorla, C.; Bogliotti, N.; Saleh, N.; Blanchard, F.; Gandon, V.; Métivier, R.; Xie, J.; Voituriez, A.; Marinetti, A. Bimetallic gold(i) complexes of photoswitchable phosphines: synthesis and uses in cooperative

catalysis. *Catal. Sci. Technol.* **2018**, *8*, 710−715. (q) Pizzolato, S. F.; Collins, B. S. L.; van Leeuwen, T.; Feringa, B. L. Bifunctional Molecular Photoswitches Based on Overcrowded Alkenes for Dynamic Control of Catalytic Activity in Michael Addition Reactions. *Chem.—Eur. J.* **2017**, *23*, 6174−6184. (r) Sud, D.; Norsten, T. B.; Branda, N. R. Photoswitching of Stereoselectivity in Catalysis Using a Copper Dithienylethene Complex. *Angew. Chem., Int. Ed.* **2005**, *44*, 2019−2021. (s) Würthner, F.; Rebek, J., Jr. Light-Switchable Catalysis in Synthetic Receptors. *Angew. Chem., Int. Ed.* **1995**, *34*, 446−448. (t) Cacciapaglia, R.; Di Stefano, S.; Mandolini, L. The Bis-Barium Complex of a Butterfly Crown Ether as a Phototunable Supramolecular Catalyst. *J. Am. Chem. Soc.* **2003**, *125*, 2224−2227. (u) Imahori, T.; Yamaguchi, R.; Kurihara, S. Azobenzene-Tethered Bis(Trityl Alcohol) as a Photoswitchable Cooperative Acid Catalyst for Morita−Baylis−Hillman Reactions. *Chem.—Eur. J.* **2012**, *18*, 10802−10807. (v) Zhao, H.; Sen, S.; Udayabhaskararao, T.; Sawczyk, M.; Kučanda, K.; Manna, D.; Kundu, P. K.; Lee, J.-W.; Král, P.; Klajn, R. Reversible trapping and reaction acceleration within dynamically self-assembling nanoflasks. *Nat. Nanotechnol.* **2016**, *11*, 82−88.

(7) (a) Qiu, Q.; Sun, Z.; Joubran, D.; Li, X.; Wan, J.; Schmidt-Rohr, K.; Han, G. G. D. Optically Controlled Recovery and Recycling of Homogeneous Organocatalysts Enabled by Photoswitches. *Angew. Chem., Int. Ed.* **2023**, *62*, No. e202300723. (b) Wei, Y.; Han, S.; Kim, J.; Soh, S.; Grzybowski, B. A. Photoswitchable Catalysis Mediated by Dynamic Aggregation of Nanoparticles. *J. Am. Chem. Soc.* **2010**, *132*, 11018−11020.

(8) (a) Chai, J.; Zhao, Y.; Xu, L.; Li, Q.; Hu, X.-Y.; Guo, D.-S.; Liu, Y. A Noncovalent Photoswitch for Photochemical Regulation of Enzymatic Activity. *Angew. Chem., Int. Ed.* **2022**, *61*, No. e202116073. (b) Ueno, A.; Takahashi, K.; Osa, T. Photoregulation of catalytic activity of [small beta]-cyclodextrin by an azo inhibitor. *J. Chem. Soc., Chem. Commun.* **1980**, 837−838. (c) Wu, P.; Xiao, R.; Zhang, C.; Zhou, L.; Luo, Q.; Xu, J.; Liu, J. Photoregulating Catalytic Activity of Cyclodextrin-Based Artificial Glutathione Peroxidase by Charged Azobenzene. *Catal. Lett.* **2010**, *138*, 62−67. (d) Park, S.; Byun, S.; Ryu, H.; Hahm, H.; Lee, J.; Hong, S. Reversibly Photoswitchable Catalysts for Olefin Metathesis Reactions. *ACS Catal.* **2021**, *11*, 13860−13865. (e) Osorio-Planes, L.; Rodríguez-Escrich, C.; Pericàs, M. A. Photoswitchable Thioureas for the External Manipulation of Catalytic Activity. *Org. Lett.* **2014**, *16*, 1704−1707. (f) Kondo, M.; Nakamura, K.; Krishnan, C. G.; Takizawa, S.; Abe, T.; Sasai, H. Photoswitchable Chiral Phase Transfer Catalyst. *ACS Catal.* **2021**, *11*, 1863−1867. (g) Kaler, S.; McKeown, P.; Ward, B. D.; Jones, M. D. Aluminium(iii) and zinc(ii) complexes of azobenzene-containing ligands for ring-opening polymerisation of ε-caprolactone and rac-lactide. *Inorg. Chem. Front.* **2021**, *8*, 711−719. (h) Hirahara, M.; Goto, H.; Yagi, M.; Umemura, Y. A multi-stimuli responsive ruthenium complex for catalytic water oxidation. *Chem. Commun.* **2020**, *56*, 12825−12828. (i) Grewal, S.; Roy, S.; Kumar, H.; Saraswat, M.; Bari, N. K.; Sinha, S.; Venkataramani, S. Temporal control in tritylation reactions through light-driven variation in chloride ion binding catalysis − a proof of concept. *Catal. Sci. Technol.* **2020**, *10*, 7027−7033. (j) Stoll, R. S.; Peters, M. V.; Kuhn, A.; Heiles, S.; Goddard, R.; Bühl, M.; Thiele, C. M.; Hecht, S. Photoswitchable Catalysts: Correlating Structure and Conformational Dynamics with Reactivity by a Combined Experimental and Computational Approach. *J. Am. Chem. Soc.* **2009**, *131*, 357−367. (k) Martinez-Cuezva, A.; Saura-Sanmartin, A.; Nicolas-Garcia, T.; Navarro, C.; Orenes, R.-A.; Alajarin, M.; Berna, J. Photoswitchable interlocked thiodiglycolamide as a cocatalyst of a chalcogeno-Baylis−Hillman reaction. *Chem. Sci.* **2017**, *8*, 3775−3780. (l) Dai, Z.; Cui, Y.; Chen, C.; Wu, J. Photoswitchable ring-opening polymerization of lactide catalyzed by azobenzene-based thiourea. *Chem. Commun.* **2016**, *52*, 8826−8829. (m) Berryman, O. B.; Sather, A. C.; Lledó, A.; Rebek, J., Jr. Switchable Catalysis with a Light-Responsive Cavitand. *Angew. Chem., Int. Ed.* **2011**, *50*, 9400−9403. (n) Neri, S.; Garcia Martin, S.; Pezzato, C.; Prins, L. J. Photoswitchable Catalysis by a Nanozyme Mediated by a Light-Sensitive Cofactor. *J. Am. Chem. Soc.* **2017**, *139*, 1794−1797. (o) Sugimoto, H.; Kimura, T.; Inoue, S. Photoresponsive Molecular Switch to Control Chemical Fixation of CO2. *J. Am. Chem. Soc.* **1999**, *121*, 2325−2326. (p) Lawrence, R. L.; Scola, B.; Li, Y.; Lim, C.-K.; Liu, Y.; Prasad, P. N.; Swihart, M. T.; Knecht, M. R. Remote Optically Controlled Modulation of Catalytic Properties of Nanoparticles through Reconfiguration of the Inorganic/Organic Interface. *ACS Nano* **2016**, *10*, 9470−9477. (q) Zhu, L.; Yan, H.; Ang, C. Y.; Nguyen, K. T.; Li, M.; Zhao, Y. Photoswitchable Supramolecular Catalysis by Interparticle Host−Guest Competitive Binding. *Chem.—Eur. J.* **2012**, *18*, 13979−13983. (r) Xie, M.; Slocik, J. M.; Kelley-Loughnane, N.; Knecht, M. R. Effect of a Mixed Peptide Ligand Layer on Au Nanoparticles for Optical Control of Catalysis. *ACS Appl. Nano Mater.* **2022**, *5*, 9379−9388. (s) Lawrence, R. L.; Hughes, Z. E.; Cendan, V. J.; Liu, Y.; Lim, C.-K.; Prasad, P. N.; Swihart, M. T.; Walsh, T. R.; Knecht, M. R. Optical Control of Nanoparticle Catalysis Influenced by Photoswitch Positioning in Hybrid Peptide Capping Ligands. *ACS Appl. Mater. Interfaces* **2018**, *10*, 33640−33651. (t) Lawrence, R. L.; Cendan, V. J.; Scola, B.; Liu, Y.; Lim, C.-K.; Prasad, P. N.; Swihart, M. T.; Knecht, M. R. Optical Control of Biomimetic Nanoparticle Catalysts Based upon the Metal Component. *J. Phys. Chem. C* **2018**, *122*, 28055−28064.

(9) (a) Wilson, D.; Branda, N. R. Turning "On" and "Off" a Pyridoxal 5′-Phosphate Mimic Using Light. *Angew. Chem., Int. Ed.* **2012**, *51*, 5431−5434. (b) Neilson, B. M.; Bielawski, C. W. Photoswitchable NHC-promoted ring-opening polymerizations. *Chem. Commun.* **2013**, *49*, 5453−5455. (c) Eisenreich, F.; Kathan, M.; Dallmann, A.; Ihrig, S. P.; Schwaar, T.; Schmidt, B. M.; Hecht, S. A photoswitchable catalyst system for remote-controlled (co)-polymerization in situ. *Nat. Catal.* **2018**, *1*, 516−522. (d) Teator, A. J.; Shao, H.; Lu, G.; Liu, P.; Bielawski, C. W. A Photoswitchable Olefin Metathesis Catalyst. *Organometallics* **2017**, *36*, 490−497. (e) Fu, C.; Xu, J.; Boyer, C. Photoacid-mediated ring opening polymerization driven by visible light. *Chem. Commun.* **2016**, *52*, 7126−7129. (f) Neilson, B. M.; Bielawski, C. W. Photoswitchable Organocatalysis: Using Light To Modulate the Catalytic Activities of N-Heterocyclic Carbenes. *J. Am. Chem. Soc.* **2012**, *134*, 12693−12699. (g) Iida, H.; Umebayashi, N.; Yashima, E. Photoswitchable organocatalysis in acylation of alcohol using dithienylethene-linked azoles. *Tetrahedron* **2013**, *69*, 11064−11069.

(10) Szewczyk, M.; Sobczak, G.; Sashuk, V. Photoswitchable Catalysis by a Small Swinging Molecule Confined on the Surface of a Colloidal Particle. *ACS Catal.* **2018**, *8*, 2810−2814.

(11) Jana, N. R.; Peng, X. Single-Phase and Gram-Scale Routes toward Nearly Monodisperse Au and Other Noble Metal Nanocrystals. *J. Am. Chem. Soc.* **2003**, *125*, 14280−14281.

(12) Sashuk, V. Thiolate-Protected Nanoparticles via Organic Xanthates: Mechanism and Implications. *ACS Nano* **2012**, *6*, 10855−10861.

(13) Schnack-Petersen, A. K.; Pápai, M.; Møller, K. B. Azobenzene photoisomerization dynamics: Revealing the key degrees of freedom and the long timescale of the trans-to-cis process. *J. Photochem. Photobiol., A* **2022**, *428*, No. 113869.

(14) (a) Pace, G.; Ferri, V.; Grave, C.; Elbing, M.; von Hänisch, C.; Zharnikov, M.; Mayor, M.; Rampi, M. A.; Samorì, P. Cooperative light-induced molecular movements of highly ordered azobenzene self-assembled monolayers. *Proc. Nat. Acad. Sci. U.S.A.* **2007**, *104*, 9937−9942. (b) Chu, Z.; Han, Y.; Bian, T.; De, S.; Král, P.; Klajn, R. Supramolecular Control of Azobenzene Switching on Nanoparticles. *J. Am. Chem. Soc.* **2019**, *141*, 1949−1960.

(15) Jatmika, C.; Wakabayashi, K.; Tamaki, R.; Akiyama, N.; Nakamura, I.; Hirota, S.; Yamaguchi, H.; Matsuo, T. Ligand Exchange Strategy for Delivery of Ruthenium Complex Unit to Biomolecules Based on Ruthenium−Olefin Specific Interactions. *Chem. Lett.* **2020**, *49*, 1490−1493.

(16) Jawiczuk, M.; Marczyk, A.; Trzaskowski, B. Decomposition of Ruthenium Olefin Metathesis Catalyst. *Catalysts* **2020**, *10*, 887.

(17) (a) Pellizzoni, E.; Şologan, M.; Daka, M.; Pengo, P.; Marson, D.; Posel, Z.; Franchi, S.; Bignardi, L.; Franchi, P.; Lucarini, M.; Posocco, P.; Pasquato, L. Thiolate end-group regulates ligand arrangement, hydration and affinity for small compounds in

https://doi.org/10.1021/acscatal.3c04435
ACS Catal. 2023, 13, 15967−15976

monolayer-protected gold nanoparticles. *J. Colloid Interface Sci.* **2022**, *607*, 1373−1381. (b) Gabellini, C.; Şologan, M.; Pellizzoni, E.; Marson, D.; Daka, M.; Franchi, P.; Bignardi, L.; Franchi, S.; Posel, Z.; Baraldi, A.; Pengo, P.; Lucarini, M.; Pasquato, L.; Posocco, P. Spotting Local Environments in Self-Assembled Monolayer-Protected Gold Nanoparticles. *ACS Nano* **2022**, *16*, 20902−20914.

(18) Mati, I. K.; Edwards, W.; Marson, D.; Howe, E. J.; Stinson, S.; Posocco, P.; Kay, E. R. Probing Multiscale Factors Affecting the Reactivity of Nanoparticle-Bound Molecules. *ACS Nano* **2021**, *15*, 8295−8305.

(19) Thiel, V.; Wannowius, K.-J.; Wolff, C.; Thiele, C. M.; Plenio, H. Ring-Closing Metathesis Reactions: Interpretation of Conversion−Time Data. *Chem.—Eur. J.* **2013**, *19*, 16403−16414.

(20) Bousquet, L.; Nicholas, K. M. In search of alkene-diazene cross metathesis. *J. Organomet. Chem.* **2019**, *899*, No. 120909.

(21) Sashuk, V.; Danylyuk, O. A Thermo- and Photo-Switchable Ruthenium Initiator For Olefin Metathesis. *Chem.—Eur. J.* **2016**, *22*, 6528−6531.

(22) Deo, C.; Bogliotti, N.; Métivier, R.; Retailleau, P.; Xie, J. Photoswitchable Arene Ruthenium Complexes Containing o-Sulfonamide Azobenzene Ligands. *Organometallics* **2015**, *34*, 5775−5784.

https://doi.org/10.1021/acscatal.3c04435
ACS Catal. 2023, 13, 15967−15976